ChemPubSoc Europe

DOI: 10.1002/chem.201600156

CHEMISTRY A European Journal Full Paper

Biosensors

Ternary Hybrid γ-Fe_2O_3/Cr^{VI}/Amine Oxidase Nanostructure for Electrochemical Sensing: Application for Polyamine Detection in Tumor Tissue

Emanuela Bonaiuto,[a] Massimiliano Magro,[a, b] Davide Baratella,[a] Petr Jakubec,[b] Elisabetta Sconcerle,[a] Milo Terzo,[a] Giovanni Miotto,[c, d] Alberto Macone,[e] Enzo Agostinelli,[e, f] Silvano Fasolato,[g] Rina Venerando,[c] Gabriella Salviulo,[h] Ondrej Malina,[b] Radek Zboril,[b] and Fabio Vianello*[a, b]

Abstract: Dichromate binds to surface-active maghemite nanoparticles (SAMNs) to form a stable core–shell nanostructures (SAMN@Cr^{VI}). The hybrid was characterized by Mössbauer spectroscopy, high-angle annular dark-field imaging, electron energy-loss spectroscopy, and electrochemical techniques, which revealed a strong interaction of dichromate with the nanoparticle surface. Electrochemical characterization showed lower charge-transfer resistance, better electrochemical performance, and more reversible electrochemical behavior with respect to naked SAMNs. Moreover, SAMN@Cr^{VI} is an excellent electrocatalyst for hydrogen peroxide reduction. Furthermore, an enzyme, namely, bovine serum amine oxidase (BSAO: EC 1.4.3.6), was immobilized on SAMN@Cr^{VI} by self-assembly to give a ternary hybrid nanostructured catalyst for polyamine oxidation (SAMN@Cr^{VI}-BSAO). SAMN@Cr^{VI}-BSAO was applied for the development of a reagentless, fast, inexpensive, and interference-free polyamine biosensor, which was successfully exploited for the discrimination of tumorous tissue from healthy tissue in human crude liver extracts.

Introduction

Hybrid nanomaterials composed of different functional components with different nanoscale functionalities have attracted increasing interest due to their combination of physical and chemical properties and potential applications in the areas of electronics, photonics, catalysis, biotechnology, nanotechnology, and biosensing.[1] In particular, bimetallic core–shell nanostructures composed of two distinct metals are emerging as a new class of materials.[2,3] Core–shell nanostructures are increasingly attracting attention because of their versatile compositions and structures, which can be applied for different purposes.[4] In addition, they not only show a combination of the properties associated with the two different metals, but, more interestingly, they display great enhancement of specific physical and chemical properties due to synergistic effects.[5,6] Recently, we developed a novel wet-synthesis pathway for producing a new type of superparamagnetic maghemite (γ-Fe_2O_3) nanoparticles, known as surface-active maghemite nanoparticles (SAMNs), which exhibited well-defined crystalline structure, peculiar surface characteristics, excellent colloidal stability, reversible direct binding properties without the necessity of any additional coating modification, and unique spectroscopic and electrochemical features.[7,8] The aim of the present work was the development of a novel electroactive surface for sensing applications in biological systems. Hence, SAMNs were coated with a chromium shell to produce a novel core–shell nanostructure, namely, SAMN@Cr^{VI}. This bimetallic core–shell nano-

[a] Dr. E. Bonaiuto, Dr. M. Magro, Dr. D. Baratella, E. Sconcerle, Dr. M. Terzo, Prof. Dr. F. Vianello
Department of Comparative Biomedicine and Food Science
University of Padua
Agripolis—Viale dell'Università 16, Legnaro, 35020 (PD) (Italy)
E-mail: fabio.vianello@unipd.it

[b] Dr. M. Magro, Dr. P. Jakubec, Dr. O. Malina, Prof. R. Zboril, Prof. Dr. F. Vianello
Regional Centre of Advanced Technologies and Materials
Palacky University, Olomouc (Czech Republic)

[c] Dr. G. Miotto, Dr. R. Venerando
Department of Molecular Medicine
University of Padua (Italy)

[d] Dr. G. Miotto
Proteomic Center of Padova University
VIMM and Padova University Hospital, Padua (Italy)

[e] Dr. A. Macone, Prof. E. Agostinelli
Department of Biochemical Sciences "A. Rossi Fanelli"
University of Rome "La Sapienza", Rome (Italy)

[f] Prof. E. Agostinelli
CNR, Institute of Molecular Biology and Pathology, Rome (Italy)

[g] Dr. S. Fasolato
Unit of Hepatic Emergencies and Liver Transplantation
Department of Medicine, University of Padua, Padua (Italy)

[h] Prof. G. Salviulo
Department of Geosciences, University of Padua (Italy)

Supporting information and the ORCID identification number(s) for the author(s) of this article can be found under http://dx.doi.org/10.1002/chem.201600156.

material was characterized by Mössbauer spectroscopy, high-angle annular dark-field imaging (HAADF), and electron energy-loss spectroscopy (EELS) for elemental mapping in a scanning transmission electron microscope in parallel with energy-dispersive X-ray spectroscopy analysis and electrochemical techniques, which revealed efficient electrocatalysis of hydrogen peroxide electroreduction and feasibility for future applications using oxidase-based biosensors.

SAMN@Cr^{VI} was further modified with bovine serum amine oxidase (BSAO) by self-assembly. This enzyme, a copper/TPQ AO, catalyzes the oxidative deamination of primary amino groups of mono-, di-, and polyamines to aldehydes, at the expense of O_2 reduction to H_2O_2. The ping-pong catalytic mechanism of copper/TPQ AOs can be divided into two half-reactions:[9] enzyme (E) reduction by the substrate at the quinone moiety (TPQ→$TPQH_2$) and its reoxidation by molecular oxygen [Eqs. (1) and (2)]

$$E_{ox} + RCH_2NH_3^+ \rightarrow E_{red}NH_3^+ + RCHO \quad (1)$$

$$E_{red}NH_3^+ + O_2 + H_2O \rightarrow E_{ox} + NH_4^+ + H_2O_2 \quad (2)$$

BSAO was able to directly bind on the SAMN@Cr^{VI} surface by self-assembly, forming an SAMN@Cr^{VI}-BSAO nanobioconjugate (SAMN@Cr^{VI}-BSAO), which was used for the development of an enzyme-based carbon-paste electrode (SAMN@Cr^{VI}-BSAO/CPE). SAMN@Cr^{VI}-BSAO/CPE was used for the development of a biosensor by using immobilized BSAO as a bioelement that produces hydrogen peroxide during the catalytic cycle.

Polyamines are ubiquitous molecules among animal and plant cells, and their content has been strongly correlated with cell growth and cancer development.[10] They are involved in numerous processes in carcinogenesis, such as cell proliferation and expression of genes responsible for tumor invasion and metastasis.[11] The high concentration of polyamines in cancer cells, as a consequence of alterations of cell metabolism, is attracting the interest of researchers studying anticancer therapies. Among all the neoplastic pathologies, hepatocellular carcinomas stand out as the third most lethal cancer worldwide.[12] SAMN@Cr^{VI}-BSAO/CPE was used for the development of a polyamine biosensor, which was successfully applied for the discrimination of tumor tissues from healthy liver by polyamine content in human crude biopsy liver extracts.

Results and Discussion

Surface coating of SAMNs with $Cr_2O_7^{2-}$

As-prepared maghemite nanoparticles can easily form colloidal suspensions when treated in an ultrasonic bath (see Supporting Information). Furthermore, as a colloidal suspension, SAMNs can be superficially modified by simple incubation in the presence of $K_2Cr_2O_7$ to form an SAMN@Cr^{VI} hybrid nanomaterial. The amount of bound chromium was determined by UV/Vis spectroscopy by monitoring the disappearance of soluble $Cr_2O_7^{2-}$ in solution. The derivatization of naked maghemite nanoparticle suspensions (500 mg L^{-1} SAMNs, 50 mL) was tested in the presence of 100 μM $K_2Cr_2O_7$ as a function of pH in the range 2.0–9.0. In particular, when the coating reaction was carried out at pH 3.0, the surface saturation coverage of SAMNs was 44 mg of $Cr_2O_7^{2-}$ per gram. Conversely, when the coating reaction was carried out at pH values higher than pH 9.0, the efficiency of the binding reaction decreased to 40% with respect to the amount of bound chromium at pH 3.0. Noteworthily, both SAMNs and SAMN@Cr^{VI} showed the same stability in water, as colloidal suspensions, up to a concentration of 1.0 g L^{-1}.

To characterize the chemical and physical interactions between iron oxide nanoparticles and chromate in the SAMN@Cr^{VI} nanoconjugate, in-field ^{57}Fe Mössbauer spectroscopy at 5 and 300 K was employed (data not shown) and values of the Mössbauer hyperfine parameters were determined. The ratio of the spectral area of the octahedral sextet to that of the tetrahedral sextet of 5:3 reflects the occupation of individual sites by Fe^{3+} ions. Taking into account the stoichiometric formula of maghemite, given by $(Fe^{3+})_T(Fe^{3+}{}_{5/3}O_{1/3})^OO_4$, where o stands for vacancies and subscripts T and O represent tetrahedral and octahedral positions, respectively, the prepared SAMN@Cr^{VI} nanoconjugate is consistent with perfectly stoichiometric maghemite, and thus chromium binding does not lead to any significant structural alteration of the iron oxide nanoparticles.

High-resolution transmission electron microscopy (HRTEM)

The morphological organization of the nanoconjugate involving SAMNs and chromium (SAMN@Cr^{VI}) is shown in the HRTEM image (Figure 1 A). From the micrograph, neither a visible alteration nor degradation of the SAMNs occurred on chromium uptake from aqueous solution. We investigated the nanoparti-

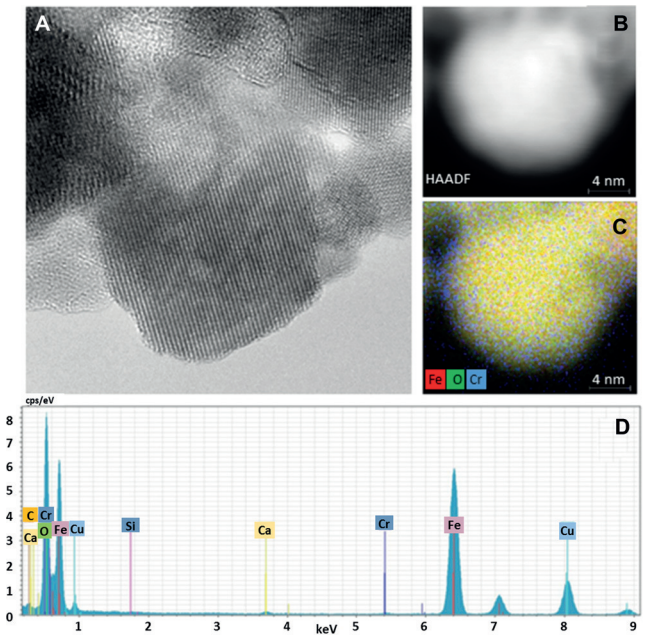

Figure 1. A) HRTEM image of SAMN@Cr^{VI}. B) HAADF analysis of SAMN@Cr^{VI}. C) STEM-EELS image of an individual SAMN@Cr^{VI} nanoparticle, showing the presence of Cr. D) EDX analysis.

cle morphology by HRTEM in environments containing different amounts of dichromate salt and at different pH (from 3.0 to 7.0). The morphology observed (in terms of the average size distribution and appearance of the nanoparticles) did not reveal substantial differences in all cases, and thus only the representative images for the system obtained at pH 3, which shows the highest degree of chromium entrapment, are reported herein. Moreover, SAMN@Cr^{VI} was characterized by HAADF and EELS for elemental mapping in a scanning transmission electron microscope (STEM; Figure 1B and C), which are highly sensitive to variations in the atomic number of atoms in the sample (*Z*-contrast images). HAADF imaging was performed in parallel with EDX analysis (Figure 1D). The Cu signal comes from the grid used to deposit the sample for the TEM study, and elements such as Si and Ca are readily detected even if present in traces in the distilled water (e.g., from silica glass and $CaCl_2$) used for nanoparticle dispersion. As shown in Figure 1D, chromium is well represented and superimposed on iron oxide nanoparticles.

Chromium distribution on the nanoparticle surface (see Figure 1C) was estimated by dissecting STEM-EELS micrographs into 1 nm^2 square areas and evaluating the Cr signals in each area with ImageJ 1.49v software (NIH, USA). The total surface area occupied by chromium in a selected 7880.0 $Å^2$ region was first assessed (see Figure S1 in the Supporting Information), and a value of about 16.0% of the analyzed image region resulted, that is, 1268.1 ± 17.5 $Å^2$.

The BET surface area of the SAMNs was determined (46.23 $m^2 g^{-1}$), and the maximum amount of bound chromium on SAMNs was assessed by Langmuir isotherm studies (44 mg g^{-1}). Thus, the average number of $Cr_2O_7^{2-}$ ions per unit area was calculated to be 1.95 $Cr_2O_7^{2-}$ ions per square nanometer, corresponding to 3.8 Cr atoms per square nanometer. Thus, the area occupied by a single chromium atom is 4.21 $Å^2$.

To reveal the position and the distribution of chromium in the sample, a grayscale threshold was used for the STEM-EELS micrographs reported in Figure S1 in the Supporting Information. The chromium signal per square nanometer was calculated (see Figure S2A in the Supporting Information), and resulted in 3.7 ± 1.1 Cr atoms per square nanometer, homogeneously distributed on the nanoparticle surface. Moreover, a circular region of interest 1.0 nm in diameter was selected in an STEM-EELS micrograph of a single SAMN, and the nearest-neighbor distance among chromium atoms on the nanoparticle surface was evaluated with ImageJ software (see Figure S2, panel B in the Supporting Information). An average minimum distance between chromium atoms of 3.9 ± 0.9 Å resulted. The average distance was not statistically different (Neuman–Keuls multiple comparison test at 0.05%) among all the analyzed 1 nm^2 areas, and this suggests that bound $Cr_2O_7^{2-}$ ions were evenly distributed on the SAMN surface.

The study on the surface distribution of chromium on the SAMNs is the key to mapping reactive iron(III) sites of the nanoparticles, since the ligand can be used as a probe for mirroring the presence of binding sites on the crystalline surface structure. Further studies are in progress to elucidate the topography of reactive iron(III) sites on the SAMN surface.

Electrochemical characterization of SAMNs and SAMN@Cr^{VI}

The electrochemical properties of the hybrid material were studied and compared with those of the naked iron oxide nanoparticles.[13,14] Thus, the electrochemical behavior of SAMN@Cr^{VI} was characterized as a function of the amount of Cr coating the nanoparticle surface. Nanoconjugates were prepared by simple incubation of SAMNs (500 mg L^{-1}) and $Cr_2O_7^{2-}$ in water, with amounts of $Cr_2O_7^{2-}$ ranging from 17 to 40 mg per gram of SAMNs. The thus-obtained self-assembled hybrid nanomaterials were used to prepare modified carbon-paste electrodes (CPEs). As already reported,[13,14] all CPEs were prepared by mixing 55 wt% graphite, 30 wt% silicone grease, and 15 wt% of the tested nanoconjugate. The CP-modified electrodes were first characterized by electrochemical impedance spectroscopy (EIS), which is a powerful tool for studying electrode-surface modifications. The impedance-plane plots (Nyquist diagrams) shown in Figure 2 are characterized by two distinct regions: 1) a semicircle at higher frequency, related to the charge-transfer resistance R_{ct} of the electrode/electrolyte interface, and 2) a linear region corresponding to semi-infinite diffusion of species at the modified electrode (Warburg region). The model circuit used in this study was a typical Randles circuit.[15,16]

The R_{ct} values of unmodified CPEs and CPEs modified with naked SAMNs were measured to be 151.2 and 129.6 Ω, respectively. A correlation between SAMN surface coating by $Cr_2O_7^{2-}$ and the electrochemical properties of the resulting nanoconjugate emerged. The R_{ct} values of CP electrodes modified with SAMN@Cr^{VI} linearly decreased as a function of Cr loading, whereby the rate of decrease of R_{ct} was approximately 5.5 Ω

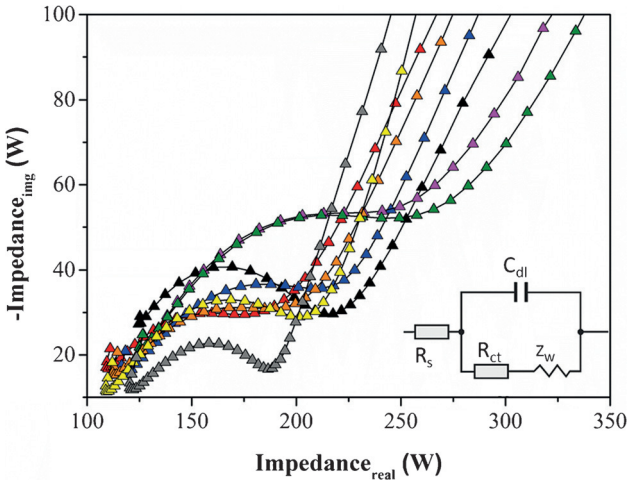

Figure 2. Nyquist plots of bare CPE, CPE modified with SAMNs, and CPE modified with SAMN@Cr^{VI}. All measurements were performed in an applied frequency range from 0.1 Hz to 100 kHz, and an ac amplitude of 5 mV was used. SAMN@Cr^{VI} was prepared by incubating naked SAMNs (500 mg L^{-1}) with different concentrations of $K_2Cr_2O_7$. Black: CPE; red: SAMN/CPE; blue: SAMN@Cr^{VI}/CPE (12 mg Cr g^{-1} SAMN); magenta: SAMN@Cr^{VI}/CPE (17 mg Cr g^{-1} SAMN); green: SAMN@Cr^{VI}/CPE (20 mg Cr g^{-1} SAMN); orange: SAMN@Cr^{VI}/CPE (23 mg Cr g^{-1} SAMN); yellow: SAMN@Cr^{VI}/CPE (33 mg Cr g^{-1} SAMN); gray: SAMN@Cr^{VI}/CPE (40 mg Cr g^{-1} SAMN). The inset shows the Randles equivalent circuit for the data fitting.

per milligram of immobilized ligand per gram of SAMNs (see Table S1 in the Supporting Information). At 40 mg of $Cr_2O_7^{2-}$ per gram of SAMN, that is, the concentration of $Cr_2O_7^{2-}$ at which the nanoparticle surface is completely saturated, R_{ct} was halved with respect to unmodified SAMNs. Moreover, the conductivity of the nanoconjugate exceeds that of the unmodified carbon matrix, and this indicates that Cr immobilization on SAMNs facilitates electron transfer between the electrode and the redox couple ($[Fe(CN)_6]^{3-/4-}$) in solution (see Table S1 in the Supporting Information). This is quite an impressive result, considering that Cr represents only 4.0% of the total weight of the nanoconjugate. Furthermore, this provides evidence of the correlation existing between the electrochemical properties of SAMNs and the reorganization of surface crystalline structure by ligand binding.

Measuring the current response of unmodified CPEs and CPEs modified with bare SAMNs in the presence of 5 mM $[Fe(CN)_6]^{3-/4-}$ resulted in values of 27.0 and 32.0 μA, respectively. The current responses of CPEs modified with the hybrid nanoconjugates prepared with amounts of $Cr_2O_7^{2-}$ ranging from 17 to 40 mg of Cr per gram of SAMN increased as a function of Cr coating. At higher $Cr_2O_7^{2-}$ concentrations, the current response followed a saturation behavior (see Figure 3).

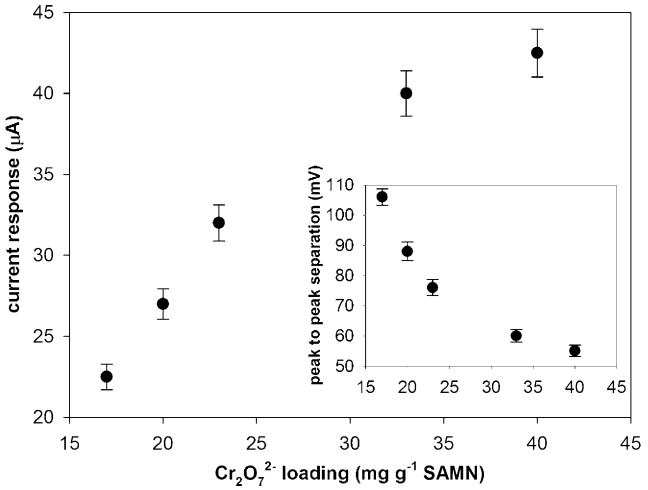

Figure 3. Current response of CPEs, CPEs modified with SAMNs, and CPEs modified with different Cr coatings on SAMNs, obtained by cyclic voltammetry. All experiments were performed in the presence of 5 mM $[Fe(CN)_6]^{3-/4-}$ at a scan rate of 50 mV s^{-1} Inset: Peak-to-peak potential for CPEs modified with different Cr coatings on SAMNs, obtained by cyclic voltammetry. For experimental details, see the Supporting Information.

At 40 mg of $Cr_2O_7^{2-}$ per gram of SAMN, that is, close to the maximum amount of bound chromium on SAMNs, the current response reached a plateau, which is further evidence of the correlation between the surface coating of the nanoconjugate and its electrochemical characteristics. In addition, studying modified CPEs by cyclic voltammetry in the presence of 5 mM $[Fe(CN)_6]^{3-/4-}$ showed that Cr immobilization on SAMNs led to a more reversible electrochemical behavior with respect to bare SAMNs. In particular, the peak-to-peak potential difference of $[Fe(CN)_6]^{3-/4-}$ decreased as function of Cr loading, and was close to 57 mV at the highest concentrations, with a tendency to ideal reversible redox behavior (see Figure 4, inset). The peak-to-peak potential of $[Fe(CN)_6]^{3-/4-}$ for unmodified CPEs and CPEs modified with bare SAMNs is quasireversible, since values of 82 and 87 mV, respectively, resulted.

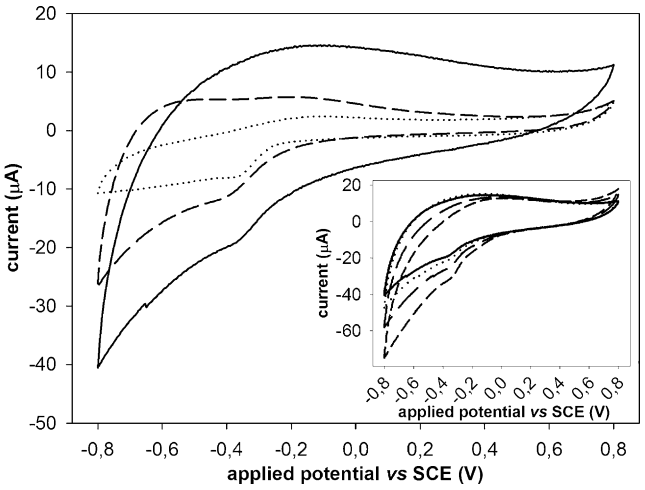

Figure 4. Cyclic voltammograms of bare CPE (dots), SAMN/CPE (short dashes), and SAMN@Cr^{VI}/CPE (solid line) at 20 mV s^{-1}, conducted in 0.1 M potassium phosphate buffer, 50 mM KCl. Inset: cyclic voltammograms of SAMN@Cr^{VI}/CPE in the presence of 1 mM (dotted), 2 mM (long dashes), and 3 mM H_2O_2 (short dashes). For experimental details, see the Supporting Information.

With occupation of the SAMN surface by Cr, the charge-transfer resistance decreased, the current response in the presence of a redox couple increased, and the system became more reversible. The modified CPs reached the ultimate electrochemical characteristics when the surface of SAMNs was completely saturated by Cr, and this indicates that Cr facilitates electron transfer when it binds on the surface of maghemite nanoparticles.

The SAMN@Cr^{VI} nanoconjugate with the highest Cr surface loading, namely, 40 mg of Cr per gram of SAMNs, was used to prepare modified CPEs, which were tested by cyclic voltammetry in the applied potential range of −0.8 to +0.8 V versus SCE, along with SAMNs/CPE and CPE. In the potential range explored, SAMNs@Cr/CPEs showed different electrochemical features with respect to SAMNs/CPE and CPE (Figure 4). In particular, a higher capacitive current, at 0.0 V versus SCE, and a higher cathodic current at negative potentials, probably due to electrocatalytic properties toward oxygen reduction, were observed.

Interestingly, as in the case of DNA binding on maghemite nanoparticles, the effect of Cr binding on SAMN recalls the electrochemical behavior produced by the introduction of an ionic liquid, namely, 1-butyl-3-methyl imidazolium hexafluorophosphate, on SAMN-modified CPEs,[17] which suggests that Cr improved the conductivity of SAMN-modified CPEs, as already described for ionic liquids.[18] These significantly altered electro-

chemical properties observed after chromium binding on SAMNs are witness to a strong interaction of dichromate with the nanoparticle surface.

Since the aim of the present work was the development of a novel electroactive surface for sensing applications in biological systems, SAMNs@Cr^{VI}/CP electrodes were characterized at neutral pH in 0.1 M phosphate buffer (pH 7.0) containing 50 mM KCl as supporting electrolyte. Furthermore, the electrocatalytic behavior of SAMNs@Cr^{VI}-modified CPEs was tested on three electroactive substances of biochemical interest, namely, hydrogen peroxide, NADH, and the hydroquinone/benzoquinone (HQ/BQ) redox couple.

Cyclic voltammetry of SAMNs@Cr^{VI}/CPEs evidenced a negligible electrocatalytic activity toward NADH and HQ/BQ (data not shown), indicating that Cr affected the electrocatalytic properties of SAMNs towards these two electroactive compounds.[13,14] Conversely, as shown in the inset of Figure 4, in the presence of hydrogen peroxide, SAMNs@Cr^{VI}/CPE showed a strong cathodic current, starting at about −0.1 V versus SCE. Moreover, the electrocatalytic performance of SAMNs@Cr^{VI}-modified electrodes were evaluated by chronoamperometry in the presence of H_2O_2, NADH, and HQ/BQ (see Table S2 and Figure S3 in the Supporting Information), and this confirmed that SAMNs@Cr^{VI}/CPE showed selectivity toward H_2O_2. The best signal-to-noise (S/N) ratio for the electroreduction of hydrogen peroxide was observed at −0.35 V versus SCE, and in the present work this potential was applied for the chronoamperometric determination of H_2O_2.

The chronoamperometric response of the SAMNs@Cr^{VI}/CPE as a function of H_2O_2 addition at an applied potential of −0.35 V is reported in Figure S3 in the Supporting Information. The calibration plot was linear (i/nA = 11.24 − 1.86 [H_2O_2]/μM, $R > 0.99$) in the range 5–500 μM. Detection limit, sensitivity, and response time were 2.47 μM, −130.25 nA μM^{-1} cm^{-2}, and 70 s, respectively (see Figure S3 in the Supporting Information). The analytical performance of this H_2O_2 sensor remained stable for at least 12 months if stored at room temperature after use. Thus, the SAMN@Cr^{VI} core–shell nanoconjugate is a stable electrocatalyst exploitable for the development of biosensors.

Immobilization of bovine serum amine oxidase on SAMN@Cr^{VI}: preparation of the ternary hybrid nanostructure

BSAO belongs to the copper-containing amine oxidase family, Cu-AO (EC 1.4.3.6), which is a heterogeneous class of enzymes widely found in mammals, plants, and microorganisms.[19] This protein, which has been characterized as a dimer with a long axis of 9.9 nm and a short axis is 6.2 nm (monomer: 762 amino acids, 84757 kDa), was immobilized on the SAMN@Cr^{VI} surface as described in the Supporting Information.

The amount of BSAO immobilized on SAMN@Cr^{VI} was determined by mass spectrometry. The mass profile of the tryptic digestion of native and SAMN@Cr^{VI}-bound enzymes yielded 57.0% sequence coverage (Figure S4 in the Supporting Information). The 15 most representative peptides, characterized by a Mascot score of greater than 35 ($P < 0.01$) and accounting for about 21.0% of the sequence coverage, were quantitatively compared to calculate the amount and specific activity of bound BSAO (Table S3 in the Supporting Information). Mass spectrometry indicated 36.7 pmol of BSAO per milligram of SAMN@Cr^{VI}.

After immobilization on SAMN@Cr^{VI}, BSAO activity was determined by measuring the rate of hydrogen peroxide production during spermine oxidation. In the case of SAMN@Cr^{VI}, no enzyme activity associated with nanoparticles was detected. The kinetic parameters, according to Michaelis–Menten, of native and immobilized BSAO are reported in Table S4 in the Supporting Information. The comparison of the enzymatic activity of native BSAO and SAMN@Cr^{VI}-BSAO under the same experimental conditions indicated that BSAO was successfully immobilized on SAMN@Cr^{VI} and showed detectable catalytic activity toward spermine ($k_{cat} = 5.28$ min^{-1}). Immobilized BSAO shows a catalytic constant of about 10.2% with respect to the native enzyme, and the Michaelis constant K_M was on the same order of magnitude as that of the native enzyme. Accordingly, the binding process led to a 2.4-fold decrease in the catalytic efficiency k_{cat}/K_M of BSAO.

SAMN@Cr^{VI}-BSAO was removed from the solution by application of an external magnet, and activity measurements were repeated with unaltered results. The SAMN@Cr^{VI}-BSAO bionanoconjugate maintains its catalytic activity over repeated washing cycles, in demonstration of the reusability of this magnetically separable nanocatalyst. The ternary hybrid nanostructure was stored in 0.1 M phosphate buffer, pH 7.0, containing 100 mM KCl, and the ferrofluid solution remained stable for at least one month.

Application of SAMN@Cr^{VI}-BSAO for polyamine biosensing

The SAMN@Cr^{VI}-BSAO ternary hybrid was used for the preparation of a biosensor by using immobilized BSAO as bioelement that produces hydrogen peroxide during the catalytic cycle, and a series of CPEs modified with SAMN@Cr^{VI}-BSAO was prepared as described in Supporting Information.

The performance of SAMN@Cr^{VI}-BSAO/CPE in the determination of H_2O_2 was evaluated by chronoamperometry at −0.35 V (vs. SCE). The modification of the SAMN@Cr^{VI} surface with BSAO did not alter significantly the analytical performance of SAMN@Cr^{VI}/CPE in H_2O_2 determination, and the electrode sensitivity and detection limit for hydrogen peroxide were unaffected. Furthermore, the response of SAMN@Cr^{VI}-BSAO)/CPE was investigated on addition of spermine as a typical BSAO substrate. In the spermine concentration range 0.1–0.70 mM, a sensitivity of 29.3 nA μM^{-1} cm^{-2} and a detection limit (S/N = 3) of 29.4 μM were calculated (see Figure S5 in the Supporting Information). The linear regression equation was: i/nA = −0.325 − 0.427 [spermine]/μM, $R = 0.998$. The stability of the (SAMN@Cr^{VI}-BSAO)/CPE was investigated, and the half-life of this reagentless polyamine biosensor was found to be longer than two months.

The development of sensing strategies that discriminate healthy and cancer tissues is a new diagnostic frontier. Thus, the proposed system was tested on healthy liver tissue samples from patients undergoing partial hepatectomy, and on

samples from patients affected by hepatocellular carcinoma, correlated to type B and C hepatitis.

The chronoamperometric response of CPE modified with the SAMN@Cr^{VI} nanoconjugate was evaluated on extracts of biopsy samples from human tumor and healthy tissues at an applied potential of −0.35 V versus SCE. No effect of interfering species on electrode response was observed. Conversely, the same measurements with CPEs modified with SAMN@Cr^{VI}-BSAO led to a current response indicating that the presence of immobilized BSAO as bioelement is uniquely responsible for the detectable electroactive species in the real samples, that is, hydrogen peroxide produced during polyamine oxidation by BSAO.

Polyamine concentrations in biopsy samples were also assessed by GC-MS (see Supporting Information). Polyamine contents determined in normal liver and in hepatocellular carcinoma samples by the biosensor and GC-MS are reported in Table 1. Both techniques gave polyamine contents in tumor tissues ($n=3$) that were about one order of magnitude higher than those in samples from healthy individuals, in agreement with the findings of Leveque and co-workers on breast cancer.[11] The polyamine concentration in the vicinity of cancer tissue is believed to play a role in cancer development. Thus, the ability to monitor polyamine moving from the tumor to adjacent regions (known as surrounding or peritumoral regions) could be an interesting task for future studies.

Table 1. Amounts of polyamine from hepatic cancer patients and healthy volunteers ($n=3$). Polyamine concentrations were determined in biopsy specimens of normal liver and hepatocellular carcinoma tissues. Data are expressed as nanograms of polyamine per milligram of tissue.

Sample	Electrochemical biosensor	GC-MS
control	434 ± 69	534 ± 16
tumoral A	1525 ± 30	993 ± 31
tumoral B	783 ± 82	700 ± 22
tumoral C	990 ± 109	729 ± 23

Conclusions

The present work has provided an example of the unpredictable properties obtainable by combining nanoparticles with different compounds in binary systems and demonstrated the possibilities offered by hybrid bimetallic nanocomposites as a tool for designing and constructing new electrochemical sensors. Previously, we reported on the presence and reactivity of solvent-exposed coordinatively unsaturated iron(III) centers on the SAMN surface as well as their proclivity to undergo electron transfer.[17,20] In the current work, an optimized procedure for the synthesis of a nanostructured SAMN@Cr^{VI} core–shell hybrid was reported, and its structural characterization was carried out by in-field Mössbauer spectroscopy, HRTEM, and elemental mapping by HAADF imaging and EDX spectroscopy. HAADF and EELS for elemental mapping in a scanning transmission electron microscope in parallel with EDX spectroscopic analysis mapped a chromium distribution mirroring the topography of iron(III) binding sites on the SAMN surface.

The electrochemical properties of the newly formed SAMN@Cr^{VI} core–shell hybrid were tested, and the electrocatalytic behavior of SAMN@Cr^{VI}-modified electrodes was studied in the presence of substances of interest for biosensing applications. The core–shell hybrid showed improved electrocatalytic performance toward H_2O_2 electroreduction with respect to bare SAMNs, which indicates electrochemical selectivity of the electrodes based on SAMN@Cr^{VI}. Furthermore, the hybrid was very stable and suitable for further functionalization and/or biomolecule immobilization. Indeed, BSAO was immobilized on the surface of SAMN@Cr^{VI}, and its biological activity was well preserved, and thus a ternary hybrid γ-Fe_2O_3/Cr^{VI}/BSAO (SAMN@Cr^{VI}-BSAO) nanostructure was successfully synthesized. Thus, the self-assembled coating of Cr^{VI} on SAMNs led to a tuning of both chemical and electrochemical properties of the iron oxide nanomaterial: the presence of chromate allowed the binding of BSAO, which does not bind spontaneously to the SAMN surface, and the electrochemical properties of the SAMNs were drastically modified on formation of the self-assembled Cr^{VI} shell.

Finally, the SAMN@Cr^{VI}-BSAO nanobioconjugate was employed for the development of an interference-free biosensor for polyamine determination in liver cancer tissues. Several studies have indicated that polyamines can be regarded as elective markers of carcinogenesis, and high polyamine concentrations were correlated with cell proliferation and increased expression of the genes responsible for tumor invasion and metastasis.[21–23] Moreover, hepatocellular carcinoma is still the third most lethal cancer worldwide.[12] We found that polyamine content was two times higher in patients affected by hepatocellular carcinoma in comparison with healthy individuals. The SAMN@Cr^{VI}-BSAO-based biosensor, which allows the simultaneous detection of total polyamines in a single measurement, is an attractive diagnostic tool for cancer monitoring.

Experimental Section

Chemicals were purchased at the highest commercially available purity and were used without further treatment. Iron(III) chloride hexahydrate (97%), potassium dichromate ($K_2Cr_2O_7$), sodium borohydride ($NaBH_4$), ammonia solution (35% in water), putrescine, spermidine, spermine, N^1-acetylspermine, 1,6-diaminohexane, ethyl chloroformate, pentafluoropropionyl anhydride, diethyl ether, ethyl acetate, and dichloromethane of pesticide grade were obtained from Sigma-Aldrich, Italy. All other chemicals were of analytical grade. Amine oxidase from bovine serum was purified to electrophoretic homogeneity according to Turini et al.[24] Enzyme samples were used with a minimum specific activity on benzylamine oxidation of 0.38 IU mg^{-1}.

Instrumentation, methods and characterization techniques are reported in the Supporting Information.

Acknowledgements

The present experimental work was partially funded by Italian Institutional Ministry grants cod. 60A06-7411 and 60A06-8055. The authors gratefully acknowledge University of Padua (Italy), grant "Assegni di Ricerca Junior" 2014 n. CPDR148959 and CARIPARO Foundation for the support. Moreover, the authors gratefully acknowledge the support from the Ministry of Education, Youth and Sports of the Czech Republic (LO1305) and the internal IGA grant of the Palacký University in Olomouc (IGA_PrF_2015_017). Thanks are also due to Regione Lazio, Prot. FILAS-RU-2014-1020 and Sapienza University Rome—Italian MIUR (EA).

Keywords: biosensors · cancer · chromium · enzymes · nanostructures

[1] V. Urbanova, M. Magro, A. Gedanken, D. Baratella, F. Vianello, R. Zboril, *Chem. Mater.* **2014**, *26*, 6653 – 6673.
[2] R. Purbia, S. Paria, *Nanoscale* **2015**, *7*, 19789 – 19873.
[3] D. Wang, Y. Li, *Adv. Mater.* **2011**, *23*, 1044 – 1060.
[4] M. B. Gawande, A. Goswami, T. Asefa, H. Guo, A. V. Biradar, D. L. Peng, R. Zboril, R. S. Varma, *Chem. Soc. Rev.* **2015**, *44*, 7540 – 7590.
[5] T. Krenke, E. Duman, M. Acet, E. F. Wassermann, X. Moya, L. Manosa, A. Planes, *Nat. Mater.* **2005**, *4*, 450 – 454.
[6] D. Xu, Z. P. Liu, H. Z. Yang, Q. S. Liu, J. Zhang, J. Y. Fang, S. Z. Zou, K. Sun, *Angew. Chem. Int. Ed.* **2009**, *48*, 4217 – 4221; *Angew. Chem.* **2009**, *121*, 4281 – 4285.
[7] M. Magro, G. Valle, U. Russo, L. Nodari, F. Vianello, 2012a. Patent no. WO 2012/010200A1.
[8] M. Magro, G. Sinigaglia, L. Nodari, J. Tucek, K. Polakova, Z. Marusak, S. Cardillo, G. Salviulo, U. Russo, R. Stevanato, R. Zboril, F. Vianello, *Acta Biomater.* **2012**, *8*, 2068 – 2076.
[9] A. Bellelli, L. Morpurgo, B. Mondovi, E. Agostinelli, *Eur. J. Biochem.* **2000**, *267*, 3264 – 3269.
[10] S. S. Cohen, *A guide to the polyamines*, Oxford University Press, New York, **1998**.
[11] J. Levêque, F. Foucher, J. Y. Bansard, R. Havouis, J. Y. Grall, J. P. Moulinoux, *Breast Cancer Res. Treat.* **2000**, *60*, 99 – 105.
[12] J. Ferlay, H. R. Shin, F. Bray, D. Forman, C. Mathers, D. M. Parkin, *GLOBOCAN* 2008 v2.0. Available from: http://globocan.iarc.fr.
[13] D. Baratella, M. Magro, G. Sinigaglia, R. Zboril, G. Salviulo, F. Vianello, *Biosens. Bioelectron.* **2013**, *45*, 13 – 18.
[14] M. Magro, D. Baratella, N. Pianca, A. Toninello, S. Grancara, R. Zboril, F. Vianello, *Sens. Actuators B* **2013**, *176*, 315 – 322.
[15] J. F. Rubinson, Y. P. Kayinamura, *Chem. Soc. Rev.* **2009**, *38*, 3339 – 3347.
[16] M. Gebala, W. Schuhmann, *Phys. Chem. Chem. Phys.* **2012**, *14*, 14933 – 14942.
[17] M. Magro, D. Baratella, P. Jakubec, G. Zoppellaro, J. Tucek, C. Aparicio, R. Venerando, G. Sartori, F. Francescato, F. Mion, N. Gabellini, R. Zboril, F. Vianello, *Adv. Funct. Mater.* **2015**, *25*, 1822 – 1831.
[18] M. Opallo, A. Lesniewski, *J. Electroanal. Chem.* **2011**, *656*, 2 – 16.
[19] "Amine oxidases": P. F. Knowles, D. M. Dooley, in *Metal Ions in Biological Systems* (Eds.: H. Sigel, A. Sigel), Marcel Dekker, New York, **1994**, pp. 361 – 403.
[20] M. Magro, D. Baratella, G. Salviulo, K. Polakova, G. Zoppellaro, J. Tucek, J. Kaslik, R. Zboril, F. Vianello, *Biosens. Bioelectron.* **2014**, *52*, 159 – 165.
[21] P. Tavladoraki, A. Cona, R. Federico, G. Tempera, N. Viceconte, S. Saccoccio, V. Battaglia, A. Toninello, E. Agostinelli, *Amino Acids* **2012**, *42*, 411 – 426.
[22] V. Vijayanathan, E. Agostinelli, T. Thomas, T. J. Thomas, *Amino Acids* **2014**, *46*, 499 – 509.
[23] E. Agostinelli, F. Vianello, G. Magliulo, T. Thomas, T. J. Thomas, *Int. J. Oncol.* **2015**, *46*, 5 – 16.
[24] P. Turini, S. Sabatini, O. Befani, F. Chimenti, C. Casanova, P. L. Riccio, B. Mondovì, *Anal. Biochem.* **1982**, *125*, 294 – 298.

Received: January 13, 2016
Published online on April 8, 2016